Proceedings of ASME Turbo Expo 2011
GT2011
June 6-10, 2011, Vancouver, British Columbia, Canada

GT2011-45882

START-UP BEHAVIOR OF A THREE-BLADED H-DARRIEUS VAWT: EXPERIMENTAL AND NUMERICAL ANALYSIS

Alessandro Bianchini **Lorenzo Ferrari** **Sandro Magnani**
"Sergio Stecco" Department of Energy Engineering, University of Florence, Florence, Italy
Tel. +39 055 4796570 - Fax +39 055 4796342 - E-mail ferrari@vega.de.unifi.it

ABSTRACT

Despite increasing attention paid by both the industrial and the academic worlds, an effective diffusion of Darrieus wind turbines is still hindered by productivity lower than that of classical HAWTs, mainly connected to the critical behavior of these machines during the transient phases and in particular, during the start-up transitory, which has not been investigated in depth in the past. In this paper, a numerical code for the evaluation of the transient behavior of H-Darrieus turbines is presented. The time-dependent code was based on a theoretical approach derived from the Momentum Models and completed by several sub-models for the evaluation of the main secondary and parasitic effects. The new software was validated with an extended experimental campaign in a wind tunnel on a three-bladed H-Darrieus turbine, obtaining constant agreement with experimental data.

A sensitivity analysis was then performed in order to investigate the start-up behavior of a generic small size three-bladed H-Darrieus rotor. In particular, for a fixed turbine layout, the influence of the airfoil type and the blade shape on the startup capabilities of the rotor was investigated as a function of the initial position of the rotor and the oncoming wind velocity.

NOMENCLATURE

A	Turbine Swept Area	[m^2]
AR	Aspect Ratio	
C_A	Equivalent Chord of the Struts	[m]
C_L	Lift Coefficient	
C_D	Drag Coefficient	
C_{thrust}	Thrust Coefficient	
C_{norm}	Normal Thrust Coefficient	
C_{tang}	Tangential Thrust Coefficient	
D	Turbine Diameter	[m]
D_T	Tower Diameter	[m]
H	Turbine Height	[m]
I_z	Momentum of Inertia	[kg·m^2]
L	Influence Length of the Tower Wake	[m]
N	Blades Number	
O_J	Centroid of the Generic Strut Portion	
P	Turbine Power	[W]
R	Turbine Radius	[m]
RPM	Round per Minute	
TSR	Tip Speed Ratio	
U	Undisturbed Wind Velocity	[m/s]
U_D	Velocity Deficit in the Wake	[m/s]
U_R	Relative Wind Velocity	[m/s]
a	Induction Factor	
b	Tower Wake Extension	[m]
c	Blade Chord	[m]
r	Local Radius	[m]
tu	Turbulence Level (%)	
x,y	General Coordinates	[m]

Superscripts

*	Dimensionless Value

Subscripts

0	Initial Value
aer	Aerodynamic
AVE	Average Value
d	Disk
par	Parasitic
REF	Reference Value
TOT	Total
WIND	Wind

Greek letters

α	Incidence Angle	[deg]
ϑ	Azimuthal Angle	[deg]
μ	Mean Wind velocity	[m/s]
ρ	Air Density	[kg/m^3]
σ	Solidity	
ω	Revolution Speed	[rad/s]

INTRODUCTION

In current wind energy research, Darrieus VAWTs are attracting interest due to the possibility of producing small machines with low visual impact and almost no noise.

In particular, increasing research efforts are being devoted to understanding where these small-size wind turbines can effectively represent an alternative for a delocalized power production and an emissions reduction, particularly when applied in new installation contexts (e.g. the built environment [1]), where the operating conditions can be very far from those of conventional wind farms.

Darrieus turbines diffusion, however, is still hampered by the generally poor performance and particularly by their start-up and transient behavior. In the past, when the Darrieus concept was only applied to big size Troposkien-bladed turbines, the start-up capabilities of these machines were not investigated in depth or even bypassed by the application of electric motors which could initially put the rotor in motion (e.g. [2]).

This approach is no longer acceptable, especially when small-power turbines are studied, in which the use of a motor/generator would imply a significant increase of the complexity of both the mechanical apparatus and the control system. In addition, the use of a motor to enable the turbine startup would have a remarkable impact on the energy yield of the turbine at the low wind speeds (note that a microeolic turbine with a nominal power of 1 kW @ 14 m/s is supposed to provide approximately 10 W @ 3 m/s).

The self-starting capability has therefore become an intrinsic requirement and theoretical and experimental research in this direction has been recently performed. Within this context, some researchers [3] stated that the Darrieus turbine is inherently non-self-starting. Conversely, others stated that self-starting is possible but only on the condition that variable geometry blades or very careful airfoil selections are adopted ([4] and [5]). More recently, Dominy et al. [6] and Hill et al. [7] demonstrated that self-starting is possible for a three-bladed H-rotor even using a fixed geometry and symmetrical airfoils, but self-starting will only occur for two-bladed designs under particular conditions. In our study, a confirmation of this latter trend is presented, based on both experimental tests in a wind tunnel and on numerical simulation carried out with a purposefully developed code. In particular, an investigation on the start-up behavior of a generic three-bladed H-Darrieus rotor was carried out, outlining the influence on the transitory of the airfoil type and the blade shape as a function of the initial position of the rotor and the oncoming wind velocity.

NUMERICAL CODE

Darrieus VAWTs have been known for many years but only recently have experienced increased interest in both experimental and numerical research. A very interesting survey on the tendencies and perspectives in the numerical modeling of VAWTs has been recently proposed by Simão Ferreira [8], who stated that, although Double Multiple Streamtubes models are currently the most widely exploited tools for the analysis and design of this turbine typology, an accurate modeling of these machines cannot disregard the most recent developments in the 2D and 3D approaches. In particular, Simão Ferreira proposed some improvements based on a 2D free-wake panel/vortex model.

In addition, CFD studies are increasingly applied to investigate in depth the complex aerodynamic phenomena which take place during a VAWT functioning, especially concerning the vortex dynamics and interactions. Within this context, however, a theoretical approach based on the so called *Blade Element Momentum (BEM) Theory* can still provide some advantages under defined circumstances, especially concerning the general design of a machine (e.g. overall dimensions and attended power) and particularly when a reduction of the computational cost is needed [2]. These latter requirements are particularly relevant in approaching the transient analysis of a turbine, in which the aerodynamic interactions must be solved instant by instant, with a sensible increase of the computational efforts.

In a BEM approach, the thrust through the rotor, which is derived from the momentum balance (2nd member of Eq. 1), is directly paired with the evaluation of the aerodynamic loads on the blades of the machine with the well-known Eqs. 1 and 2:

$$C_{thrust} = \frac{U_R^{\,2} Hc\left(-C_{norm}\sin\vartheta + C_{tang}\cos\vartheta\right)}{AU^2} = 4a(1-a) \quad \textbf{(1)}$$

$$\begin{cases} C_{norm} = -C_L\cos\alpha - C_D\sin\alpha \\ C_{tang} = C_L\sin\alpha - C_D\cos\alpha \end{cases} \quad \textbf{(2)}$$

The influence of relevant design parameters can be straightforwardly estimated with this method, especially as regards the effect of the aerodynamic characteristics of the airfoils, which are particularly critical in the evaluation of the startup transitory.

Furthermore, focusing on the analysis of a transitory, in which continuous changes in the blade working conditions are implied, although no significant approximations are introduced by the inadequate description of the wake and vortex interactions using a BEM model, great advantages can nevertheless be derived from the possibility of directly calculating the blade torque as a function on the azimuthal position and the revolution regime of the rotor (Eq. 3).

$$T_{blade}(\vartheta) = \frac{1}{2}\rho c\int_H U_R^{\,2} C_{tang} r(h)dh \quad \textbf{(3)}$$

Moving from this theoretical background, the numerical code for the analysis of the transient behavior of the turbines was developed using a simplified approach based on the Momentum Models; in detail, in order to overcome the limits of previous examples found in the technical literature [6], the application was conceived as a direct subroutine of the main VARDAR code of the University of Florence (Refs. [9-11]), in order to exploit its accurate description of the aerodynamic flow field around the turbine. The VARDAR code makes use of a *Double Multiple Streamtubes (DMS) approach*, as originally proposed by Paraschivoiu [12]. The calculation of the induced velocities through the rotor exploits the principle of the two actuators disks in tandem [13]; as a result, different induction factors are found in the upwind and in the downwind section of the turbine. The variation in the interference factors with the azimuthal angle ϑ is also considered (i.e. the induced velocities change with respect to ϑ) (*Double Multiple Streamtubes with Variable interference factors* [14]) (Figure 1).

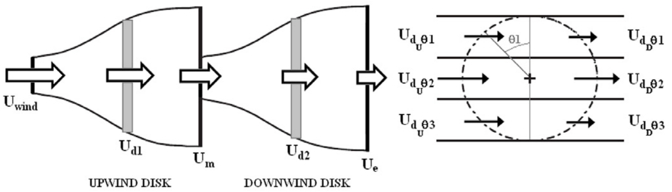

Figure 1 - DMS approach with Variable interference factors.

The Glauert's correction for the BEM theory has been taken into account with the most recent improvements based on experimental data [15], together with the corrections due to blades finite Aspect Ratio, using the Lanchester-Prandtl model [16]. In order to increase the accuracy of the aerodynamic estimations, a specific sub model to account for the dynamic stall has been provided, following the Paraschivoiu's adaptation to the DMS approach described in [2]; at the same time, the stream tube expansion along the flow path was considered with the simplified scheme presented in Ref. [2], although its incidence on the performance estimation of small turbines like those investigated in this work is reduced.

Several secondary effects have been included in the performance analysis, as well, due to the remarkable influence of these contributions to the power output of small machines [10, 14]: in particular, original models have been developed for the evaluation of the shadow effect of the central tower and the estimation of the parasitic torque of the struts [10].

The model of the tower wake (Figure 2) was derived by a simplified approach presented by Paraschivoiu [14], which was integrated with a new correlation (Eq. 4) based on experimental data [17], which significantly reduced the computational efforts with no decrement in the accuracy. The parasitic torque generated by the struts during the revolution is evaluated with a simplified model which represents an evolution of the original model proposed by Paraschivoiu for Troposkien-bladed turbines [14]; in particular, the Paraschivoiu's approach assumes the tangential velocity to represent the only component to produce drag and moreover considers a constant equivalent drag coefficient for all the rotational regimes. This scheme appears to be reductive in H-Darrieus, in which the struts have a radial extension equal to the turbine radius, and particularly in small size turbines, where the relative impact of the parasitic torque of the struts is increased [11].

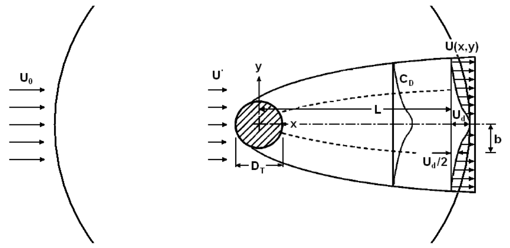

Figure 2 - Tower wake model.

$$U(x,y) = U'\left(1 - 1.2\left(C_{DT}\frac{D_T}{x}\right)^{\frac{1}{2}}\right)e^{\left(\frac{-13y^2}{C_{DT}D_T x}\right)} \qquad \textbf{(4)}$$

For all these reasons, a more sophisticated scheme (Figure 3) was developed to account for the resistant torque of the struts. By exploiting the Multitubes approach, the relative velocity on the struts in the new model is punctually evaluated as a function of the absolute wind velocity, the azimuthal angle and the local radius for each rotational speed. In addition, in the present model the Drag coefficient is given as a function of both the struts cross section and the relative Reynolds Number. Based on these hypotheses, the average parasitic torque of a rotating strut at a given TSR (i.e. a given ω) is given by Eq. 5, where C_A is the equivalent chord of the strut.

$$T_{AVE}(\omega) = \frac{1}{4\pi}\rho C_A \int_0^{2\pi}\int_{D_T/2}^{R} C_D(\omega,\vartheta,r)\cdot U_R(\vartheta,r)^2\, dr\, d\vartheta \qquad \textbf{(5)}$$

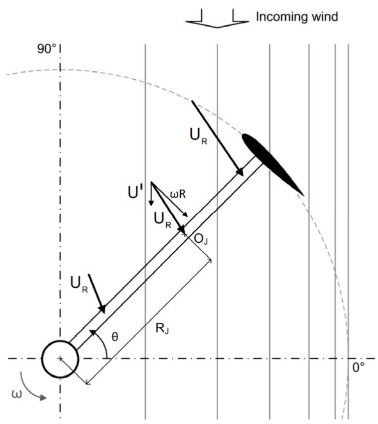

Figure 3 - Struts model.

The numerical tool for the evaluation of the transient behavior was in particular conceived as a direct subroutine of the main VARDAR code. After the solution of the aerodynamic field around the turbine, the master code releases a set of matrices to the subroutine, each of which contains the overall torque value of a single blade as a function of the TSR and ϑ for a fixed wind velocity. For example, a 2D visualization of a torque matrix, in terms of dimensionless torque ($T^*=T/T_{REF}$), is shown in Figure 4, in which one can readily appreciate that the torque production is primarily located in the upwind half of the revolution, having its maximum in terms of average output in a revolution at a TSR=2.2 (whereas the maximum power output for the same turbine is shifted to the slightly higher TSR=2.5, being $P=T\omega$). The torque matrices are created for the desired range of wind velocities and TSRs. Furthermore, torque maps with the same structure are also created by the master code for the parasitic torques, that mainly come from the aerodynamic resistance of the blades supports and the tie-rods [10] and from the parasitic torques of the bearings and the generator.

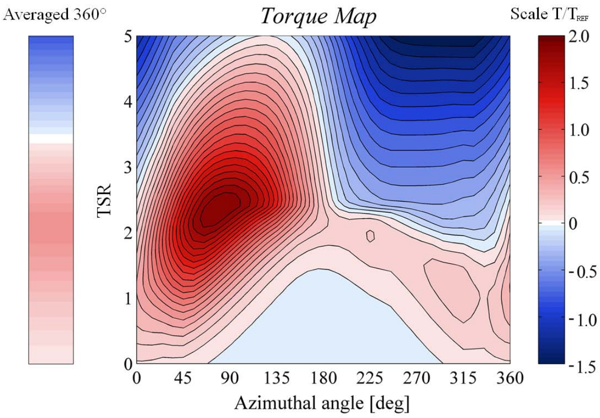

Figure 4 - 2D visualization of a torque map.

Starting from these input parameters and from some boundary conditions (i.e. initial turbine positioning and revolution speed), the time-dependent code, instant by instant, solves the equation of the uniformly accelerated motion: the net torque value at each instant (i.e. the overall torque of the blades minus the overall parasitic torque) is determined by an interpolation within the two matrices, corresponding to the actual wind velocity and using the values of the angle and TSR calculated at the end of the previous iteration (Eq. 6). In case of wind changes, a further interpolation is required between the right matrices of the wind velocity.

$$T_{TOT}(\vartheta, TSR) = \sum_{i=1}^{N} T_{aer_i}(\vartheta, TSR) - \sum T_{par}(\vartheta, TSR) \qquad \textbf{(6)}$$

In addition, a new model to account for the *virtual camber effect* [18] was implemented. The virtual camber effect in VAWTs is a complex aerodynamic phenomenon connected to the curved path that is followed by the blades: in detail, the curved path causes a variation of the real incidence angle on the airfoil (*virtual incidence*) and a variation in the flow field which the airfoil itself is immersed in: this variation can be also described as a virtual variation of the airfoil shape (*virtual camber*). To account for this effect at the functioning regime, a counter-modification of the camber line of the airfoils embedded on H-Darrieus turbines is often provided ([10] and [18]). In the startup phase, however, where blades are at rest or in slow motion, the virtual camber effect has a different influence on the blade performance; in detail, in our code, the virtual camber effect has been neglected in the first part of the accelerating ramp (i.e. the lift and drag coefficient of the geometric airfoil are used) and then applied when the blades are rotating faster than a peculiar regime. Thanks to an analogy with helicopter aerodynamics, the transition point was chosen at the rotational speed in which the time needed by a particle of air to cover a linear path equal to the blade chord becomes longer than the time needed by the turbine to sweep the circular arc subtended to the blade chord itself. The model has been experimentally validated, obtaining a constant agreement between numerical estimations and experimental data [19].

In conclusion, the developed code ensures the possibility to investigate the startup behavior of a generic turbine as well as any other transient phenomenon like wind gusts or slopes. The main advantages of this approach, compared to other proposed simulation tools (e.g. [6]) is that very small computational efforts are required during the iterations because the aerodynamic flow conditions on the blade in each time instant are no longer solved during the iteration itself; in addition, a more accurate evaluation of both the aerodynamics and the parasitic torque can be achieved by the exploitation of a fully developed DMS approach. Some precautions are required however: the transient study of such a complex machine is greatly dependent both on the correct evaluation of the aerodynamic performance of the airfoils (i.e. lift and drag coefficients in the 0°-360° range) and on the accurate description of the geometrical and massive features (e.g. the momentum of inertia).

EXPERIMENTAL CAMPAIGN

The numerical code has been validated with several experimental campaigns that were carried out by the authors using the testing facilities of the wind tunnel of the Federico II University of Naples (Italy). In the 3x3 m squared section of the gallery a maximum velocity of 50 km/h can be reached with a turbulence level of approximately 0.5%.

H-Darrieus models with either two straight blades (Figure 5 sx) or three (helix shaped) blades Darrieus turbine (Figure 5 dx), have been tested, whose main characteristics are reported in Table 1 and Table 2. The turbines were connected to an electric motor/brake which was used to explore the entire power curve of the machine. The torque and turbine revolution velocities were measured with a high precision torque meter.

The proper corrections of the velocity modulus of the oncoming flow on the turbine due to the section blockage (approximately 8.2% for the two-bladed model and 12.5% for the three-bladed model) were applied, by taking into account both the solid and the wake blockage, as prescribed by Refs. [20-21] in case of complex geometries (e.g. VAWTs).

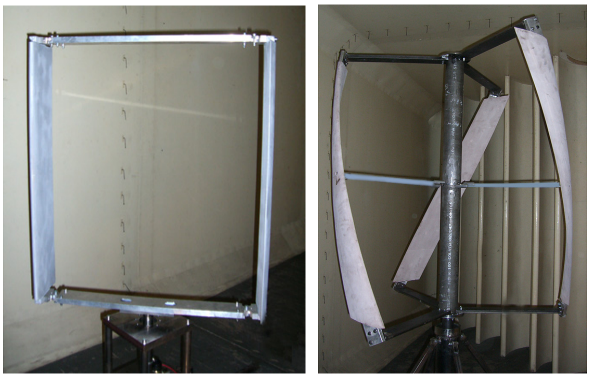

Figure 5 - Sx: Two-bladed model; Dx: Equivalent prototype of the three-bladed model (the real rotor - entirely built in plastic with shaped struts - cannot be shown due to the industrial copyright).

Table 1 - Main characteristics of the two-bladed model.

Blades Number		2
Blades Shape		straight
Blades Airfoil		Custom - lightly cambered
Diameter (D)= Height (H)	[m]	1.0
Chord (c)	[m]	0.2
AR_{blade}		5.0
Solidity (σ)		0.4
Momentum of Inertia (I_z)	[kg·m^2]	10.8

Table 2 - Main characteristics of the three-bladed model.

Blades Number		3
Blades Shape		helix 60°
Blades Airfoil		Custom - lightly cambered
Diameter (D)= Height (H)	[m]	1.45
Chord (c)	[m]	0.22
AR_{blade}		6.6
Solidity (σ)		0.45
Momentum of Inertia (I_z)	[kg·m^2]	7.6

Several transient tests were also performed in the wind tunnel only on the three-bladed turbine, which represented a real pre-industrial prototype, with its final shape and building material (plastic). During all the tests, the turbine was allowed to rotate freely around its axis (i.e. the electrical system was disconnected). The revolution signal was obtained by an optic sensor which was installed in front of the shaft base of the machine, viewing a reflective strip positioned on the shaft itself; the reflective strip was then related to the angular position of a master blade, in order to investigate the influence of the starting angle of the turbine on the acceleration ramp.

A notable agreement was constantly found between the numerical estimations and the experimental data, both concerning the power curves of the machines obtained with the VARDAR code (e.g. Figures 6 and 7, where the power outputs are presented in a dimensionless form $P^*=P/P_{REF}$ to preserve a non-disclosure agreement with our industrial partner) and the startup ramps, which were simulated with the numerical model presented in this study (e.g. Figures 8 and 9); in particular, the time-dependent code was able to correctly predict both the total time of the acceleration and the shape of the ramp. A slight discrepancy between the predicted and experimental values in the low revolution velocities range occurs only for the velocity of 3 m/s, mainly due to the lack of lift and drag coefficients data for these low-Reynolds cases.

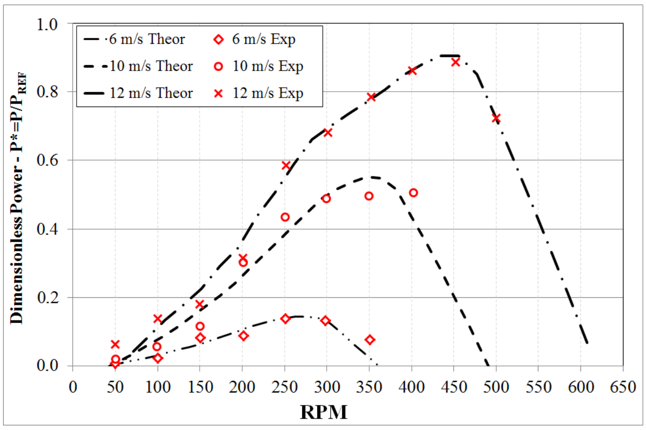

Figure 6 - Comparison between numerical estimations and experimental data: power curves of the two-bladed model.

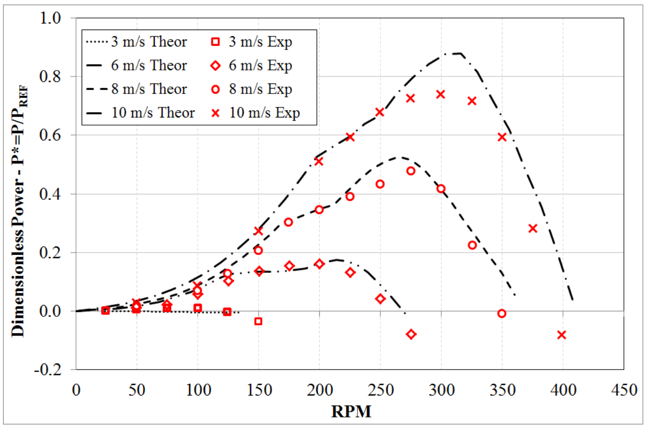

Figure 7 - Comparison between numerical estimations and experimental data: power curves of the three-bladed model.

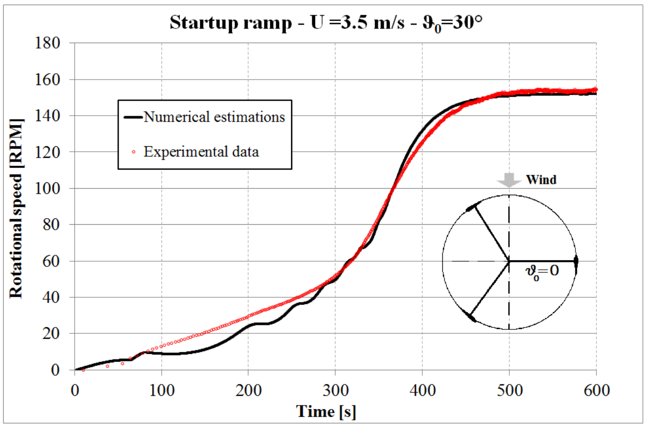

Figure 8 - Comparison between numerical estimations and experimental data: startup ramp @ U=3.5 m/s and ϑ_0=30°.

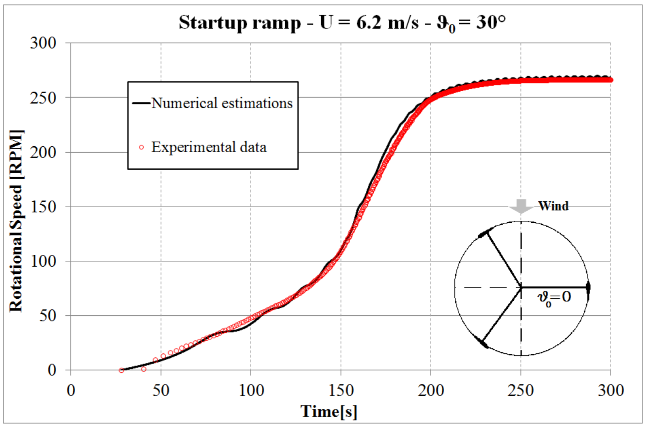

Figure 9 - Comparison between numerical estimations and experimental data: startup ramp @ U=6.2 m/s and ϑ_0=30°.

In addition, it is worth noticing that the measured startup behavior was always slightly smoother than the computed one, as a result of the fact that the numerical simulations are based on a discrete time-steps discretization each of which implies specific interpolations on the aerodynamic data, whereas the real functioning of the turbine is characterized by a continuous and progressive variation of the aerodynamic conditions. In addition, damping sources connected to the mechanical chain cannot be modeled accurately in the numerical model.

SELF-STARTING BEHAVIOR OF A THREE-BLADED TURBINE: GENERAL ASPECTS

The term "self-starting", with reference to a Darrieus turbine, needs to be defined carefully. Ebert and Wood [22] define the starting process as having been completed when a significant power extraction is allowed, whereas Kirke [5] deems a turbine to be self-starting only if it can accelerate from rest to the point where it starts to produce a useful output.

As correctly highlighted by Dominy et al. [6], however, in both of the previous cases, the definitions of the terms "significant power" and "useful output" are themselves imprecise. Others (e.g. Lunt [6]) adopted a more specific definition, by which a turbine is considered to have started if it has accelerated from rest to a condition where the blades operate at a steady speed that exceeds the wind speed (i.e. TSR> 1, where the machine can no longer be operating entirely as a drag device). Although more precise, this definition also has its limitations. In particular, evidence was found that reaching the point at which the blades begin to produce lift over a significant part of a revolution does not guarantee that the machine will to continue to accelerate (e.g. [23]).

In this study, a turbine is deemed to be self-starting if it can accelerate, under fixed wind conditions, to its free-run velocity in these conditions, which actually means that the turbine can entirely follow its corresponding torque (or power) curve. If these requirements are fulfilled, a classical startup curve has the shape presented in Figure 9. The physics of self-starting can, however, be more precisely understood coupling the transient response of the machine with its performance in terms of torque output: an example of this analysis is presented in Figure 10, with reference to the turbine described in Table 1 under a stable wind velocity of 3 m/s. Examining Figure 10, one may obtain a confirmation that, if the turbine is able to self-start and accelerate under the considered conditions and no load is imposed, the revolution speed at the equilibrium is the free-run velocity of the machine, i.e. the revolution regime in which the torque curve vs. RPM intersects the zero axis.

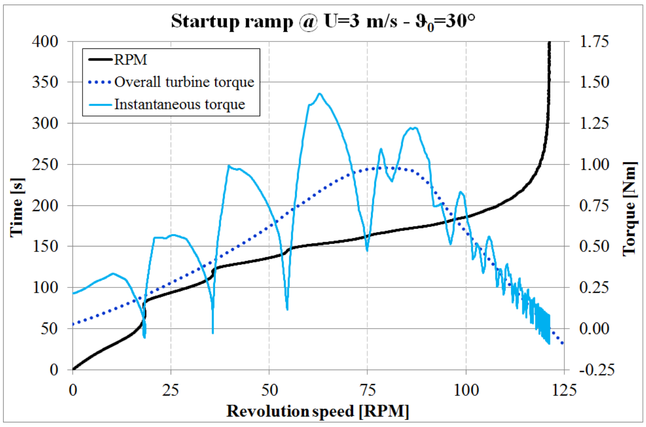

Figure 10 - Startup ramp compared to the expected torque output of the machine @ U=3.0 m/s and ϑ_0=30°.

It is also worth noticing that, comparing the nominal torque curve (i.e. the mean torque over a revolution) and the torque values during the transitory, some intensive ripples are predicted. These ripples, mainly located in the left half of the curve, are due to the inertia of the rotor, as confirmed by the analysis presented in Figure 11, where the startup ramp of the turbine is compared with the hypothetic ramps of the same machine having the momentum of the inertia halved or doubled, respectively. By reducing the inertia of the rotor, a faster acceleration can be obtained: the torque ripples in the transitory are less intense and fewer; by increasing the inertia, the torque peaks become more intense and more frequent.

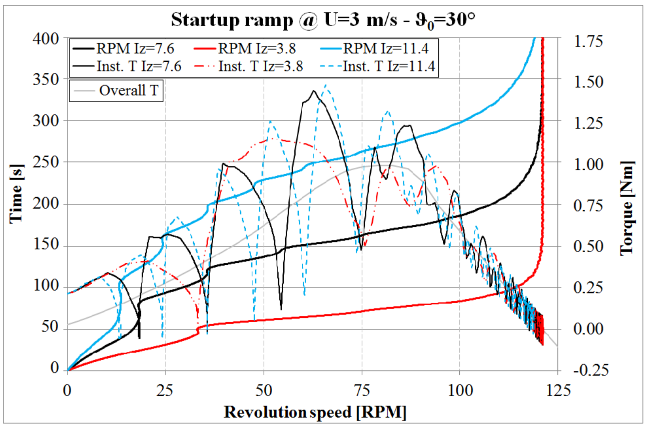

Figure 11 - Startup ramp and torque output of the machine @ U=3.0 m/s and ϑ_0=30° for different values of the rotor inertia.

Although the presented criterion is very useful for understanding the physics of the self-starting, it must be highlighted that, in the case of industrial machines, a modification of the criterion is probably required by taking into account the load that the electric control system will impose to the machine when it reaches the design operating point for the analyzed wind velocity. For example, in Figure 12 the hypothetic startup ramp of the turbine is reported in case the nominal load is required by the electric system whenever the turbine passes the nominal rotational speed in the torque curve for the investigated wind velocity (i.e. 88 RPM). Within an industrial application, if no change in the wind occurs, the turbine would continue to rotate at the nominal velocity with the correct power production; conversely, whenever a lack of load occurs (e.g. a failure of the control system) the machine would complete its acceleration to the free-run velocity.

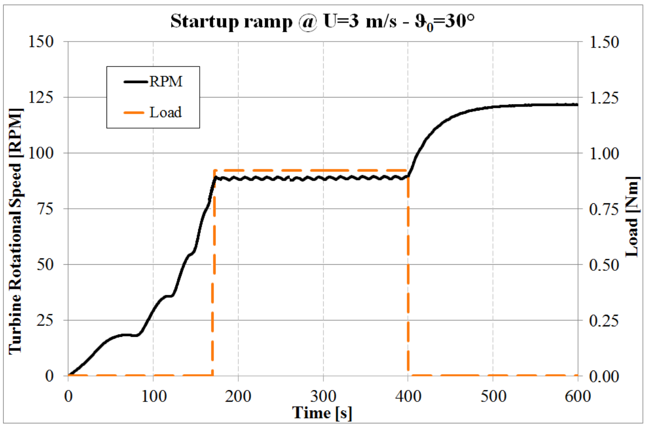

Figure 12 - Startup ramp with a variable load applied.

The described self-starting behavior of a fixed-pitch Darrieus rotor is however strictly dependent on the turbine geometry and mass features and from its initial positioning, as well. From a theoretical point of view (i.e. a model based only on the aerodynamics), as already noticed by Hill et al. [7] and Dominy et al. [9], some particular positioning of the machine, especially if straight-bladed, can prevent the self-starting.

In particular, a straight-three-bladed Darrieus turbine has been frequently supposed to be unable to self-start for low wind velocities if its initial position is near to ϑ_0=0° (see Figure 13) or ϑ_0=90°. The 0° positioning is a particular aerodynamic condition where the combination of lift coefficients of the three blades results in a very low total torque of the machine, which can actually prevent the motion of the turbine (e.g. Figure 13); conversely, the 90° positioning (see Figure 15) is a singular condition affected by theoretical fluctuations of the turbine near the equilibrium (e.g. Figure 14).

These aerodynamic singularities are however bypassed in the real functioning by both the intrinsic unsteadiness of the real wind and by the geometrical asymmetries of the machines which allow the two critical positions [11] to be overcome. In confirmation of this evidence, in Figure 13 and 15 are reported the effects of a 20° wind shift on the theoretical self-start behavior of a three-straight-bladed turbine with the same geometrical features of Table 1. As one may notice, a simple wind shift (frequent in the real functioning) can make the turbine escape from the singular positioning and ensure the self-starting.

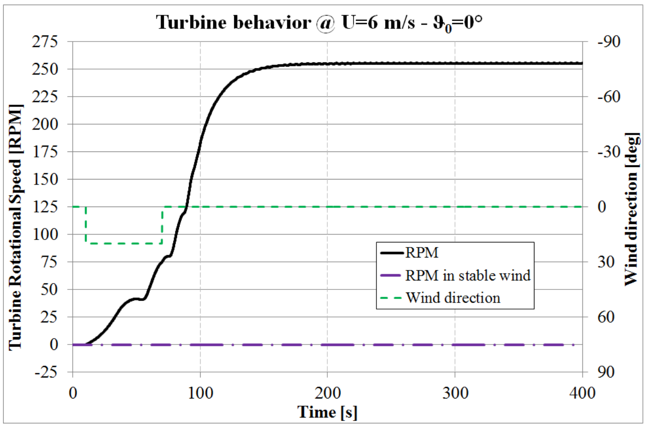

Figure 13 - Effect of a variation in the wind direction on the theoretical startup behavior of the machine @ ϑ_0=0°.

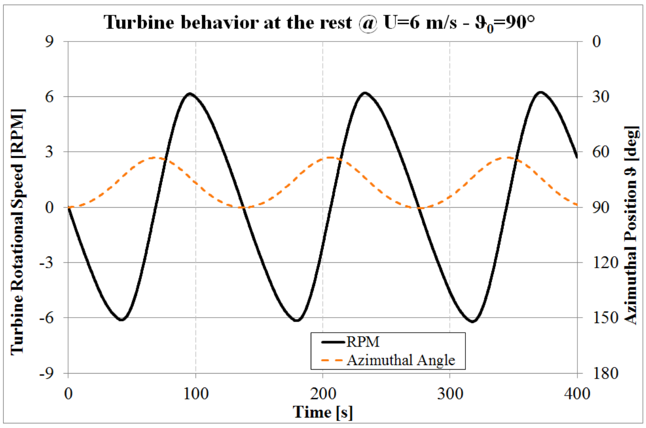

Figure 14 - Theoretical behavior of a three-blade turbine with straight blades at the rest @ ϑ_0=90°.

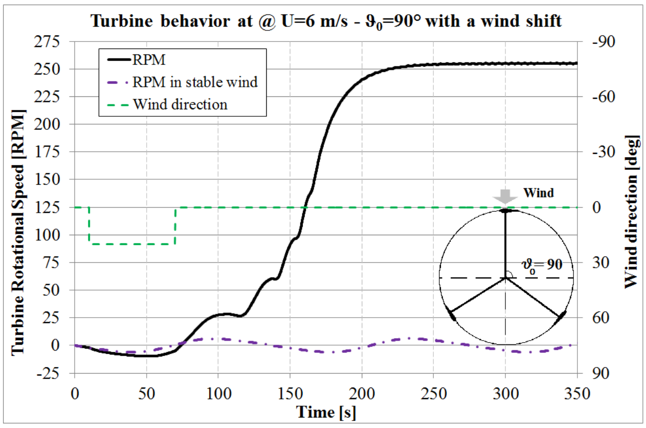

Figure 15 - Theoretical behavior of a three-blade turbine with straight blades @ ϑ_0=90° when a wind shift occurs.

In addition, other peculiar effects are introduced in the startup functioning of the turbine by the real wind conditions.

For example, if one considers the turbine at rest with no wind, the effective self-starting of the machine is greatly influenced by the raise trend of the wind, which is generally very far from an impulsive form. In confirmation of this effect, in Figure 16 is reported the comparison between the startup trends of a turbine ideally invested by a 6 m/s constant wind and that of a turbine which experiments a linear-raising wind: a notable delay is here introduced by the wind raise due to the slowing down of the accelerating ramp in the first part of the curve (i.e. when the rotational regime is increasing slowly).

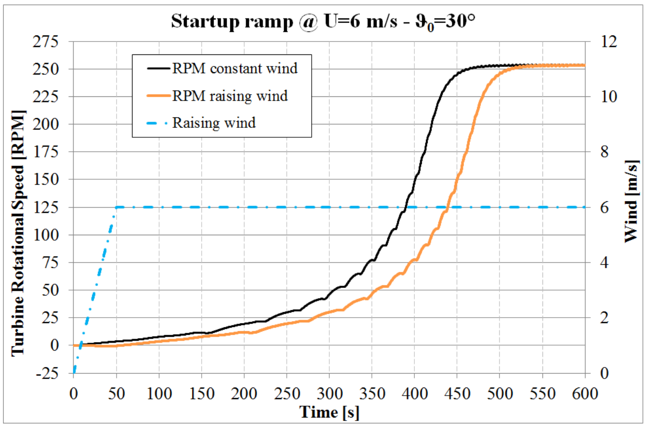

Figure 16 - Effect of the raise trend of the wind.

Finally, the effects of the wind macro-turbulence have to be taken into consideration. The real wind turbulence can indeed modify the starting time of the machine and even determine a different free-run velocity due to the regulating problems that are generated whenever velocity modulus variations during time are given (e.g. see Figure 17).

The combined effects of a real-type wind (e.g. μ=3 m/s linearly increasing, tu=10%, periodic wind direction shifts of 15°) on the startup behavior of the turbine (geometrical features from Table 1 starting from ϑ_0=30°), are presented in Figure 18.

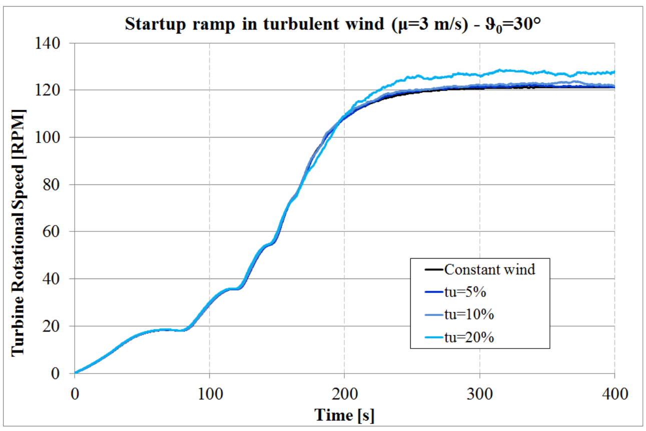

Figure 17 - Effect of the wind turbulence.

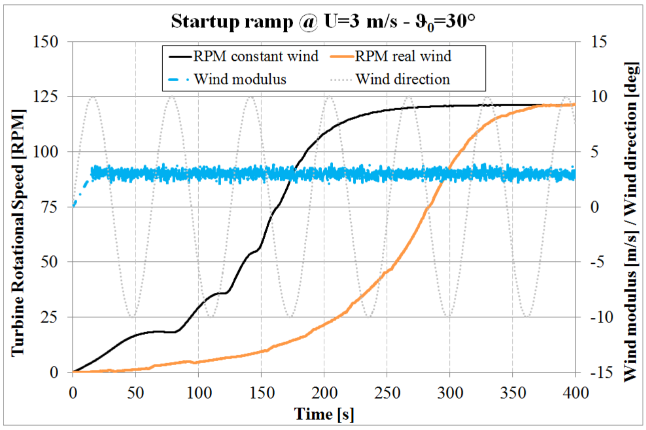

Figure 18 - Effect of a real-type on the startup of the turbine.

EFFECTS OF THE BLADE SHAPE AND THE AIRFOIL TYPE ON THE SELF-STARTING CAPABILITIES

A sensitivity analysis was performed in order to evaluate some general trends in the startup behavior of a three-bladed H-Darrieus turbine as a function of the airfoil type (i.e. symmetric, NACA0015, or lightly cambered, NACA4415) and the blade shape (i.e. straight or helix-shaped with an helix angle of 60°).

With reference to a hypothetic turbine with the geometrical features described in Table 1, for which a large amount of experimental data were collected during the wind tunnel campaign, the variations in the self-starting behavior induced by the aforesaid design parameters were numerically evaluated for different wind velocities. The main results of the analysis are reported in Table 3 (grey cell = no expected startup).

Table 3 - Startup behavior of a three-bladed H-Darrieus turbine with different blade shapes and airfoil types.

	Wind velocity [m/s]							
Geom. conf.	2,0		3,0		5,5		6,0	
Not cambered Straight blade	θ_0=0°	θ_0=30°			+/-10° 650 s	750 s 242 RPM	+/-10° 450 s 254 RPM	490 s 254 RPM
	θ_0=60°	θ_0=90°			750 s 242 RPM	820 s 242 RPM	490 s 254 RPM	500 s 254 RPM
Not cambered Helix blade					760 s 242 RPM	710 s 242 RPM	500 s 254 RPM	485 s 254 RPM
					750 s 242 RPM	860 s 242 RPM	500 s 254 RPM	520 s 254 RPM
Cambered Straight blade	+/-15° 500 s 80 RPM	420 s 80 RPM	+/-15° 315 s 121 RPM	305 s 121 RPM	+/-15° 21 s 231 RPM	205 s 231 RPM	+/-15° 160 s 254 RPM	150 s 254 RPM
	520 s 80 RPM	+/-25° 540 s 80 RPM	325 s 121 RPM	+/-25° 325 s 121 RPM	205 s 231 RPM	+/-25° 220 s 231 RPM	180 s 254 RPM	+/-25° 160 s 254 RPM
Cambered Helix blade	+/-10° 540 s 80 RPM	510 s 80 RPM	+/-10° 400 s 121 RPM	345 s 121 RPM	+/-10° 220 s 231 RPM	220 s 231 RPM	+/-10° 200 s 254 RPM	190 s 254 RPM
	580 s 80 RPM	+/-20° 600 s 80 RPM	410 s 121 RPM	+/-20° 400 s 121 RPM	260 s 231 RPM	+/-20° 240 s 231 RPM	210 s 254 RPM	+/-20° 220 s 254 RPM

Upon examination of Table 3, some interesting trends can be highlighted:

- The airfoil choice has capital relevance in the transient behavior of the turbine (e.g. see [10] and [11]). Despite a lower overall power production at the design point, lightly cambered airfoils (like that tested in this study) can indeed provide a significant increase in the starting torque, with an impressive reduction of the starting times with respect to a symmetric airfoil (e.g. see Figure 19).
- A symmetric profile has a critically lower performance at low wind velocities (i.e. low Reynolds numbers), with a resulting cut-in velocity for the investigated machine of 5.5 m/s against the 2 m/s of the same turbine with lightly cambered airfoils. When the oncoming wind velocity is sufficiently high, however, almost no sensitivity to the initial positioning angle was found (e.g. Figure 20), with the only exception of the 0° (± 10°) position for a straight-bladed turbine. In the authors' experience, however, the aerodynamic singularity is bypassed in the real functioning.

The cambered airfoil shows remarkable accelerating capabilities for all the investigated wind velocities (e.g. see Figure 19) with a more critical behavior around ϑ_0=0° (±15°) or ϑ_0=90° (±20°). Experimental evidence showed however that an almost uniform behavior for all the initial positioning is obtained in real turbines [10]: in particular, the bold-bordered cases were verified by the authors during the wind tunnel tests.

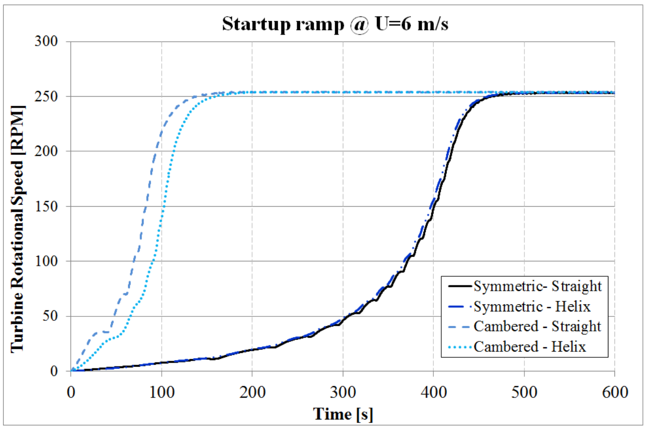

Figure 19 - Effect of the blade shape and airfoil type @ U=6 m/s, ϑ_0=30°.

- Under the same conditions in terms of the profile type, whenever the turbine is initially positioned in a favorable angle (e.g. ϑ_0=30°), the straight-bladed model has slightly lower accelerating times due to the higher efficiency of the blades (Figure 15).
- The helix-shaped blades ensure a more constant startup time for all the initial positions and can actually avoid the starting problems at ϑ_0=0°, in case a conventional symmetric profile is embedded.

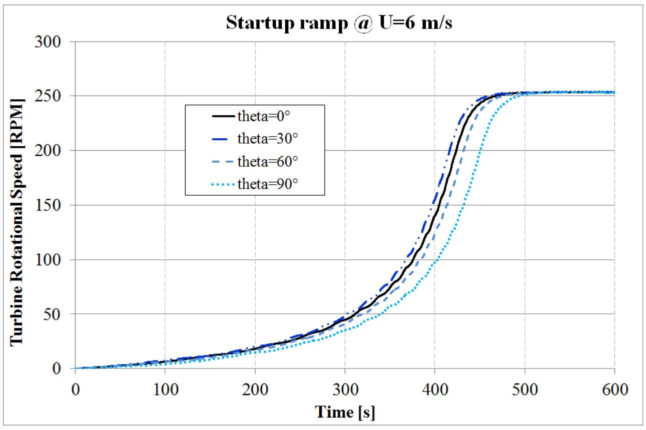

Figure 20 - Effect of the initial positioning @ U=6 m/s.

- Moreover, under the same conditions in terms of inertia of the rotor, the helix-shaped blades ensure lower torque ripples during the accelerating ramps (Figure 21) thanks to the resulting flatter torque profile of the machine (Refs. [10] and [11]). In addition, a reduction of the aerodynamic "dead bands" around ϑ_0=0° and ϑ_0=90° is gained with respect to the straight-bladed solution.

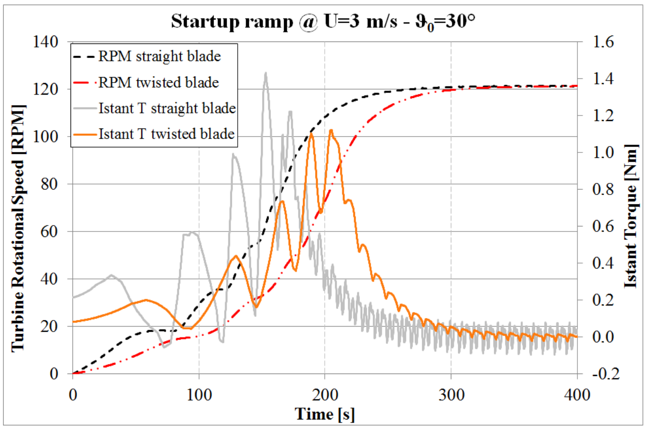

Figure 21 - Effect of the blade shape on the torque needed to complete the acceleration.

CONCLUSIONS

In this study a numerical code for the evaluation of the transient behavior of H-Darrieus turbines under generic wind conditions in terms of velocity and direction was presented.

The time-dependent code was based on a theoretical approach derived from the Momentum Models and consequently completed by several sub-models for the evaluation of the main secondary and parasitic effects. The new software was validated with an extended experimental campaign in a wind tunnel on a three-bladed H-Darrieus turbine, obtaining constant agreement with experimental data.

A theoretical analysis was then performed in order to provide a characterization of the self-staring behavior of a small-size Darrieus turbine. In the first part of the analysis, some general aspects connected to the self-starting of these turbines were examined by means of the numerical code.

For a fixed turbine layout, the influence of the airfoil type and the blade shape on the startup capabilities of the rotor was then investigated as a function of the initial position of the rotor and the oncoming wind velocity. In particular, the variations in the self-starting behavior induced by the airfoil type (i.e. symmetric or lightly cambered) and the blade shape (straight or helix-shaped with an helix angle of 60°) were numerically analyzed in a continuous relationship with experimental experience.

ACKNOWLEDGMENTS

Thanks are due to Prof. Ennio Antonio Carnevale of the University of Florence for supporting this activity. The authors would like also to acknowledge Prof. Andrea Arnone for the helpful discussion and his precious contribution to the aerodynamic study.

REFERENCES

[1] Mertens, S., 2006, *Wind Energy in the Built Environment*, Multi-Science, Brentwood, U.K. .

[2] Paraschivoiu, I., 2002, *Wind Turbine Design with Emphasis on Darrieus Concept*, Polytechnic International Press, Canada.

[3] Kentfield, J.A.C., 1996, *The fundamentals of wind-driven water pumpers*, Taylor and Francis, London, U.K. .

[4] Pawsey, N.C.K., 2002, "Development and evaluation of passive variable-pitch vertical axis wind turbines," PhD Thesis, School of Mechanical and Manufacturing Engineering, The University of New South Wales, Australia.

[5] Kirke, B.K., 1998 "Evaluation of self-starting vertical axis wind turbines for stand-alone applications", PhD Thesis, School of Engineering, Griffith University, Australia.

[6] Dominy, R., Lunt, P., Bickerdyke, A. and Dominy, J., 2007, "Self-starting capability of a Darrieus turbine," *Proc. IMechE 221 Part A: Journal of Power and Energy*, pp. 111-120.

[7] Hill, N., Dominy, R., Ingram, G. and Dominy, J., 2009, "Darrieus turbines: the physics of self-starting;" *Proc. ImechE 223 Part A: Journal of Power and Energy*, pp. 21-29.

[8] Simão Ferreira, C.J., 2009, "The near wake of the VAWT: 2D and 3D views of the VAWT aerodynamics," PhD Thesis, Technische Universiteit Delft, The Netherlands.

[9] Bianchini, A., Ferrari, L. and Schneider, A., 2008, "First steps in the design and optimization of Darrieus VAWTs for microeolic applications," *Proc. World Renewable Energy Congress (WREC) X*, Glasgow, Scotland, 19-25 July 2008.

[10] Bianchini, A., Ferrari, L. and Magnani, S., 2010, "Analysis of the Influence of Blade Design on the Performance of an H-Darrieus Wind Turbine," *Proc. ASME-ATI-UIT 2010 Conference on Thermal and Environmental Issues in Energy Systems*, Sorrento, Italy, 16-18 May 2010.

[11] Ferrari, L. and Bianchini, A., 2010. "Critical aspects in the design of a small-size Darrieus wind turbine," *Proc. World Renewable Energy Congress (WREC) XI*, Abu Dhabi, UAE, 25-30 September 2010.

[12] Paraschivoiu, I., 1981, "Double-Multiple Streamtube Model for Darrieus Wind Turbines," *Proc. 2nd DOE/NASA Wind Turbines Dynamics Workshop*, NASA CP-2186, Cleveland, USA, 24-26 February 1981, pp. 19-25.

[13] Healey, J.V., 1981, "Tandem-disk theory - With particular reference to vertical axis wind turbines," Journal of Energy, **5**, pp. 251-254.

[14] Paraschivoiu, I. and Delclaux, F., 1983, "Double Multiple Streamtube Model with Recent Improvements," Journal of Energy, **7**(3), pp. 250-255.

[15] Marshall, L. and Buhl Jr., J., 2005, "A New Empirical Relationship between Thrust Coefficient and Induction Factor for the Turbulent Windmill State," Report NREL/TP-500-36834, National Renewable Energy Laboratory, CO, USA.

[16] Abbott, I.H. and Von Doenhoff, A.E., 1959, *Theory of Wing Sections*, Dover Publications Inc., New York, USA.

[17] Blevins, R. D., Forces on and Stability of a Cylinder in a Wake, Journal of Offshore Mechanics and Arctic Engineering, Vol. 127, 2005.

[18] Migliore, P.G., Wolfe, W.P. and Fanucci, J.B., 1980, "Flow Curvature Effects on Darrieus Turbine Blade Aerodynamics," Journal of Energy, **4**(2), pp. 49-55.

[19] Bianchini, A., Carnevale, E.A. and Ferrari, L., 2010, "A Model to Account for the Virtual Camber Effect on the Performance Prediction of an H-Darrieus VAWT Using the Momentum Models," Paper submitted to Wind Engineering, pending paper n° S1252

[20] Barlow, J.B., Rae Jr., W.H. and Pope, A., 1999, *Low-speed Wind Tunnel Testing*, Wiley-Interscience Publication, New York, USA, pp. 367-375.

[21] Ross, I.J., 2010, "Wind Tunnel Blockage Corrections: an Application to Vertical-Axis Wind Turbines", Master of Science Thesis, Dayton University, Dayton (OH), USA.

[22] Ebert, P.R. and Wood, D.H., 1997, "Observations of the starting behaviour of a small horizontal-axis wind turbine," Renewable Energy, **12**(3), pp. 245–257.

[23] Baker, J. R., 1983, "Features to aid or enable self-starting of fixed pitch low solidity vertical axis wind turbines," Journal of Wind Engineering and Industrial Aerodynamics, **15**, pp. 369–380.

